CREEP PROPERTIES OF POLYCRYSTALLINE Al_2O_3 – BASED CERAMIC COMPOSITES

F.A. Huamán-Mamani[1] and M. Jiménez-Melendo[2]

[1] Universidad Católica San Pablo, Quinta Vivanco s/n, Urb. Campiña Paisajista, Arequipa, Peru (fhuaman@ucsp.edu.pe)
[2] Universidad de Sevilla, Departamento de Física de la Materia Condensada, 41012 Sevilla, Spain (melendo@us.es)

Keywords: Creep, Superplasticity, Alumina, Zirconia, Ceramic composites

ABSTRACT

Three-phase Al_2O_3 - ZrO_2 - Er_2O_3 composites with the ternary eutectic composition were fabricated by a conventional solid-state reaction route starting from commercial powders of alumina, erbia and monoclinic zirconia. Bulk composites with relative densities higher than 98% were obtained after calcining at 1400 ºC for 10 h in air and sintering at 1500 °C in air for 10 h. X-ray diffraction and energy-dispersive X-ray spectroscopy showed the presence of the three expected phases: alumina, EAG and zirconia. The composites exhibit a homogeneous microstructure with equiaxed grains of about 1 μm in size. Mechanical tests were carried out in compression at temperatures between 1300 – 1450 °C in air. Extended steady states of deformation were attained without macroscopic damage. The stress exponent in such experimental conditions was close to 2, suggesting that grain boundary sliding is the main deformation mechanism, as found in other fine-grained ceramics.

1 INTRODUCTION

There is currently a large and growing need in the industry for advanced materials with improved properties at elevated temperatures. Alumina-based composites stand out among this kind of materials, in particular for structural applications. Although monolithic alumina is inherently brittle, with a low fracture toughness at low and high temperatures [1], its mechanical properties can be considerably enhanced by the incorporation of other ceramics in composite structures (fibers, particulates, layers, etc.). For example, dual phase Al_2O_3-ZrO_2 composites (zirconia-toughened alumina, ZTA) show, relative to their single-phase counterparts, enhanced fracture resistance and strength at room temperature as well as remarkable resistance to coarsening at elevated temperatures, which has been exploited to achieve superplasticity [2-4]. In the same manner, dual phase Al_2O_3-YAG composites also exhibits superior creep resistance than their constituents [5] due to the mutual insolubility, high chemical stability and restrained grain growth of the alumina phase.

This is also the case of directionally solidified Al_2O_3-based ceramics in the eutectic composition (DSE), which show good structural stability and a high fracture strength up to temperatures close to the eutectic point [6-8]. This behaviour derives from the special lamellar microstructures obtained during solidification. In particular, directionally-solidified Al_2O_3-YAG-ZrO_2 eutectic composites have been shown to have a fracture toughness as high as 8 $MPa.m^{1/2}$ at room temperature, and the retention of large flexural, tensile and compressive strengths up to temperatures close to the eutectic temperature [6,7]. Conventional monolithic materials, however, generally do not cover the current requirements because the processing routes necessary to produce DSE ceramics are not suitable for mass production and components with custom shapes and sizes. These crystals have therefore been gradually displaced by multicomponent materials with singular microstructures. Nevertheless, the mechanical properties at elevated temperatures of sintered Al_2O_3-based composites with compositions similar to the eutectic materials are still lacking. In the present study, the mechanical response at high temperatures of polycrystalline Al_2O_3 - ZrO_2 - Er_2O_3 composites with the eutectic composition produced by conventional ceramic processing has been investigated. X-ray diffraction has been used systematically to identify the crystalline phases and their volume fractions.

2 EXPERIMENTAL PROCEDURES

2.1. Starting materials

Polycrystalline Al_2O_3-$Er_3Al_5O_{12}$(EAG)-ZrO_2 composites were produced by using conventional solid-state reaction route and high-temperature sintering. The starting high-purity commercial powders were: Al_2O_3 (99.99% purity, Sigma-Aldrich), Er_2O_3 (99.99% purity, Sigma-Aldrich) and monoclinic ZrO_2 (99.99% purity, Sigma-Aldrich). Appropriate amounts of these powders were ball-milled in agate media for 1 h using a planetary ball mill. The resulting powder mixtures were calcined at different temperatures between 1200 and 1600 °C in air for 10 h and reground again to eliminate possible agglomerates. Calcination temperatures of 1600 °C were initially selected in order to eliminate possible intermediate phases formed during the process [9]. X-ray structure analyses were systematically performed on the calcined powders in order to ensure the presence of the required phases, Al_2O_3, EAG and Er_2O_3-stabilized ZrO_2. The resulting powders were analysed by X-ray diffraction for determining the crystalline phases present in the material. Laser diffraction, using a Malvern Mastersizer 2000, was performed for particle size analysis, using distilled water as carrier medium. After that, the powder mixtures were uniaxially pressed at 150 MPa into 20-mm diameter pellets and then isostatically cold pressed at 210 MPa. The resulting green pellets were sintered in air at 1500 °C for 10 h with low heating and cooling rates (5 °C/min). The bulk density of the composites was determined from weight/dimensions measurements. The sintered samples were again analysed by X-ray diffraction looking for possible modification in crystal phases.

2.2. Microstructural and mechanical characterization

X-ray powder diffractograms were obtained using a Bruker D8 Advance A25 X-ray diffractometer with Cu Kα radiation and Ni filter, equipped with a scintillation detector in θ – 2θ Bragg-Bentano configuration (X-ray Laboratory, CITIUS, University of Sevilla, Spain). A continuous scan mode was used to collect 2θ data in the 10 – 120° range in steps of 0.015° and a scanning speed of 1.8 °/min. Collected X-ray spectra were processed by Rietveld refinement method using the TOPAS 4.2 Bruker AXS software package to quantify the nature and amount of the different crystalline phases in the powders.

The microstructural characterization of as-sintered and deformed composites was carried out using high-resolution scanning electron microscopy (HRSEM), particularly in back-scattered electron image mode to discern the different crystalline phases, and transmission electron microscopy (TEM) (Microscopy Service, CITIUS, University of Sevilla, Spain). In order to reveal the grain boundaries for SEM observations, sections were cut from the samples and mechanically polished using up to 0.25 μm-grade diamond paste, and then thermally etched at 1300 °C for 2 h in air. The relevant morphological parameters, grain size d (taken as the equivalent planar diamenter) and form factor F, were measured by using a semiautomatic image analyser. Thin films for TEM observations were obtained from the as-fabricated and deformed samples following a classical procedure of grinding and ion-thinning until electron transparency of sliced sections. Elemental composition analysis was performed by energy dispersive X-ray spectroscopy (EDS) in both SEM and TEM to characterize the various phases present in the composites.

Prismatic specimens of about 5 x 3 x 3 mm in size were cut from the sintered pellets with a low-speed diamond saw and used for mechanical experiments. Compression tests were carried out in air at temperatures T between 1300 and 1450 °C. Deformation experiments were performed under constant load in a creep machine, at nominal stresses σ between 50 and 120 MPa, and at constant cross-head speed in an universal testing machine at different initial strain rates. The recorded data, load vs. time, were analyzed in σ - ε curves, where σ and ε are the true stress and the true strain, respectively.

The mechanical data were analyzed using the standard high-temperature power law for steady-state deformation [10]:

$$\dot{\varepsilon} = A\sigma^n \exp(-Q / RT) \quad (1)$$

where A is a parameter depending on the deformation mechanism, n is the stress exponent, Q is the activation energy for creep and R is the gas constant. The parameters n and Q are characteristics of the

deformation mechanism, and were measured from stress and temperature changes, respectively, during a test on the same sample (differential method). The specimens were typically deformed to total strains of 50-60 % (unless premature failure occurred) for subsequent microstructural observations.

3 RESULTS AND DISCUSSION

Table 1 shows the particle size characteristics (in volume and in number) measured by laser diffraction of: (i) as-received powder mixtures; and (ii) ground, calcined and reground powder mixtures. There is a size reduction between the original and final powders, resulting in an average final particle size of 0.8 μm before the sintering process.

	As-received powder		Calcined and reground powder	
	volume	number	volume	number
d(0.1)	2.1	0.8	0.1	0.6
d(0.5)	6.7	1.1	1.7	0.8
d(0.9)	18.4	2.7	5.2	1.5

Table 1: Characteristic sizes d(0.1), d(0.5) and d(0.9) of the as-received powder mixtures and after ground, calcining and second ground powder mixtures.

The X-ray patterns of the calcined powders were rather complex because up to seven different phases could be identified depending on the calcination temperature. The diffraction peaks were indexed according to reference patterns of the database PDF-2002 (International Centre for Diffraction Data, ICDD) compiled in Table 2. Once the crystalline phases were identified, the Le Bail method was initially used to refine the fundamental parameters of the different diffractograms, which were subsequently refined by the Rietveld technique, allowing the quantification of the volume fractions of the various phases present in the materials.

XRD pattern	Material	Space group	Lattice parameters			
			a (Å)	b (Å)	c (Å)	β (º)
PDF-05-0712	Al_2O_3	R-3c (167)	4.758		12.991	
PDF-43-1007	Er_2O_3	Ia3 (206)	10.5480			
PDF-36-0420	m-ZrO_2	P21/c (14)	5.1463	5.2135	5.311	99.2
PDF-32-0013	$Er_4Al_2O_9$ (EAM)	P21/a (14)	7.341	10.396	11.058	108.58
PDF-24-0396	$ErAlO_3$(EAP)	Pbnm (62)	5.162	5.326	7.359	
PDF-32-0012	$Er_3Al_5O_{12}$(EAG)	Ia3d (230)	11.994	-	-	
PDF-78-1307	$Zr_{0.80}Er_{0.20}O_{1.90}$	Fm-3m (225)	5.145	-	-	

Table 2: XRD reference patterns of database PDF-2002 (International Centre for Diffraction Data, ICDD) used in this work.

In the as-ground powder, the three original phases, alumina, erbia and monoclinic zirconia were identified, indicating that no additional phases formed during the milling process. After calcination at 1200 °C, seven different phases were detected: Al_2O_3, Er_2O_3, monoclinic and cubic ZrO_2, and the three phases of the Al_2O_3-Er_2O_3 system: EAM (monoclinic), EAP (orthorhombic) and EAG (cubic). By analogy with the ternary system Al_2O_3-Y_2O_3-ZrO_2, which has been thoroughly analysed [11-13], the presence of these phases in the calcined powders can be understood if the ternary system Al_2O_3-Er_2O_3-ZrO_2 is considered to be formed by three binary systems: Al_2O_3-Er_2O_3, Er_2O_3-ZrO_2.and Al_2O_3-ZrO_2. Then, the reactions leading to the formation of the various phases can be written in the following form: in the system Al_2O_3-Er_2O_3:

$$\begin{aligned} 2Er_2O_3 + Al_2O_3 &\rightarrow Er_4Al_2O_9 \\ Er_4Al_2O_9 + Al_2O_3 &\rightarrow 4ErAlO_3 \\ 3ErAlO_3 + Al_2O_3 &\rightarrow Er_3Al_5O_{12} \end{aligned} \quad (2)$$

and in the system Er_2O_3-ZrO_2:

$$\begin{aligned} ZrO_2 + mEr_2O_3 &\rightarrow Zr_{1-x}Er_xO_{2-x/2} \\ x = 2y/1+y, \;\; y &= m/100 \end{aligned} \quad (3)$$

The latter equation denotes the structural transformation of the zirconia phase, changing from monoclinic to tetragonal or cubic structure depending on the amount of dopant ions.

As the calcination temperature increases, the intermediate monoclinic EAM and orthorhombic EAP phases disappear gradually. At 1400 ºC, only the final phases of the ternary system: alumina, EAG and zirconia, are present in the compounds; higher calcination temperatures practically do not introduce further phase changes. Regarding the zirconia phase, there is an evolution from monoclinic to cubic structure, with a final erbium ion content of 0.24 at.%, corresponding to an erbia molar concentration of 13.6 mol%. This value is close to those reported for directionally solidified AEZ eutectics grown from the melt trough different techniques [8,14]. There is no further evolution of the crystallographic phases with the sintering process. Taking into account these results, the volume fractions of the alumina, EAG and erbia-stabilized cubic zirconia in the sintered material were 42, 40 and 18 vol.%, respectively.

Fig. 1 depicts representative SEM micrographs of the as-sintered polycrystals. Fig. 1(a) is a secondary electron SEM image of a polished and thermally-etched cross-section showing a homogeneous distribution of equiaxed grains, with little porosity mainly located at triple grain junctions. Fig. 1 (b) shows the same image but in backscattered SEM mode. The alumina phase (dark phase) is easily distinguishable in this image mode, but the other two EAG and ESZ phases are hardly discerned even in this mode. They had to be identified individually by energy dispersive X-ray microanalysis.

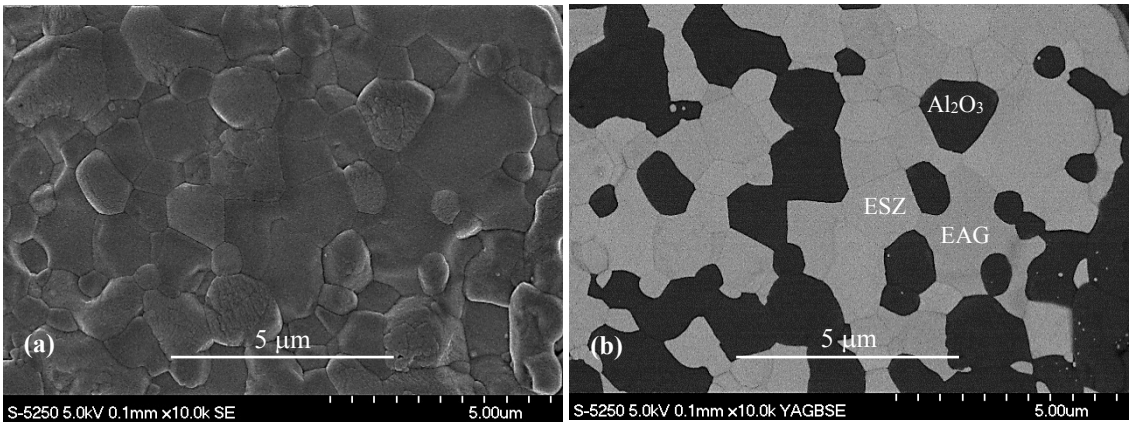

Figure 1: Microstructure of the sintered eutectic-composition Al_2O_3-EAG-ZrO_2 composite: (a) secondary electron SEM micrograph; (b) backscattered electron SEM micrograph of the same area showing the three phases: Al_2O_3 (dark), EAG and cubic ZrO_2; these latter two phases had to be identified by EDS.

The characteristic morphological parameters of the EAZ composites were: form factor F = 0.8 ± 0.1 for the three phases, indicating a regular grain growth during sintering; and grain size d = 1.1, 1.1 and 0.9 μm for Al_2O_3, EAG and Er_2O_3-ZrO_2 phases, respectively. The corresponding grain size distributions are very similar for the three phases, and could be well described by a log-normal law, as found in many ceramic materials.

TEM observations indicated that the grain boundaries are facetted and free of second phases. No dislocations activity was observed except for occasional dislocation arrays in the larger alumina and

EAG grains. These defects may be attributed to the compressive residual stresses generated upon cooling from the sintering temperature by the mismatch in thermal expansion coefficients between the alumina and the other two phases, particularly zirconia, along with the inherent anisotropy in the thermal expansion of alumina.

The average bulk density of the sintered composites was 5410 kg/m^3. The theoretical density, calculated from the expected phase composition, is 5500 kg/m^3. The following densities for individual phases have been used: 3990 kg/m^3 for alumina, 6380 kg/m^3 for EAG and 6670 kg/m^3 for cubic zirconia. The relative density of the sintered composites is thus higher than 98%, in agreement with SEM observations.

Fig. 2 displays the true stress σ – true strain ε curves of the sintered composites deformed at temperatures between 1300 and 1450 °C, for an initial strain rate $\dot{\varepsilon} = 2x10^{-5}$ s^{-1}. There is a transition from a brittle to ductile behavior with increasing temperature. At 1300 °C, the sample failed catastrophically after reaching a maximum stress of 450 MPa, with little plastic deformation. At 1400 °C and above, the composites underwent very large plastic deformation, exceeding 50% of strain without signals of macroscopic failure. In this ductile regime, the slope of the $\sigma - \varepsilon$ curves are rather constant, indicating the attainment of a steady state of deformation. The continuous shortening of the sample during a constant cross-head speed test in compression, which monotonically increases the instantaneous strain rate with respect to the initial one, is responsible for the slightly positive slope of the $\sigma - \varepsilon$ curves; such a slope increases with increasing initial strain rate and/or decreasing temperature. At the intermediate temperature of 1350 ºC, the stress – strain curve exhibits a continuous decrease of stress with strain after the yield point, indicating a progressive degradation of the composite by creep damage. It should be noted that, despite this softening, the compound still retains a relatively high strength (compared to the yield stress) at the completion of the test (ε = 50%). The transition brittle-ductile is displaced to lower temperatures as the initial strain rate decreases, and vice versa.

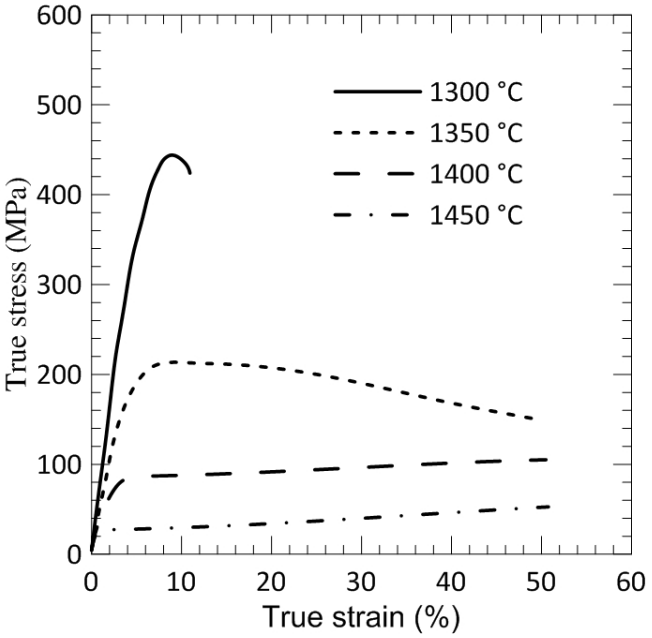

Figure 2: True stress against true strain curves for sintered Al_2O_3-EAG-ZrO_2 composites as a function of the temperature obtained at an initial strain rate of $2x10^{-5}$ s^{-1}.

Regarding the microstructure of the strained composites, there were not significant changes in the shape and size of the grains with respect to the unstrained samples in the ductile region, despite the large strains attained. Consequently, the grains had to slide on each other along their boundaries to accommodate the macroscopic strain without deformation of the grain themselves. This deformation mechanism of grain boundary sliding has been reported in other fine-grained metals and ceramics

[3,4,15], in which superplasticity has been observed.

In order to verify mechanically that grain boundary sliding was the main deformation mechanism operating in the composites in steady state conditions, creep tests at constant load were performed to determine the stress exponent n of the creep equation (Eq. 1), which characterize the deformation mechanism. An average value of the stress exponent $n = 1.9 \pm 0.2$ was measured from up- and down-load changes. This result is very close to the value of $n = 2$ systematically reported in the creep of fine-grained metals and ceramics [3,4,15] where grain boundary sliding is the dominant deformation mechanism. This is also the value predicted by most theoretical and semiphenomenological models developed to explain the superplastic behavior of fine-grained materials [4], which are based on diffusion and/or dislocation slip and climb. In addition, TEM studies revealed that there was little or no increase in dislocation activity in the deformed samples; only the larger alumina grains showed some dislocations networks forming subgrain boundaries. The ensemble of experimental features found in this study in steady state conditions supports that the creep of sintered eutectic-composition Al_2O_3–EAG–ESZ composites takes place by grain boundary sliding.

As the temperature decreases, the local stresses generated during grain boundary sliding can no longer be fully accommodated by diffusion processes, and cavities appear along the grain boundaries. These cavities eventually coalesce into cracks as the temperature further decreases, leading to sample failure.

4 CONCLUSIONS

Sintered Al_2O_3-$Er_3Al_5O_{12}$-ZrO_2 composites with the ternary eutectic composition have been successfully fabricated by a conventional solid-state reaction route, starting with high-purity commercial powders of Al_2O_3, Y_2O_3 and monoclinic zirconia as precursors. X-ray diffraction studies of calcined powders showed that the final phases: Al_2O_3, EAG and Er_2O_3 fully-stabilized cubic zirconia, without other intermediate phases, were obtained at calcination temperatures of 1400 °C. Bulk composites with a relative density higher than 98% were obtained after sintering at 1500 °C in air for 10 h. The microstructure is formed by a homogeneous distribution of equiaxed grains with average sizes of about 1 μm for the three phases.

Compressive mechanical tests were performed at constant cross-head speed and at constant load in air at high temperatures. At temperatures above 1350 ºC, extended steady states of deformation were attained without signals of macroscopic failure. In these conditions, no noticeable changes in grain morphology was detected, suggesting that grain boundary sliding was the main operating deformation mechanism. This conclusion was also supported by an experimental stress exponent of nearly 2 and the absence of dislocation activity. As the temperature decreases, a gradual transition towards a brittle behavior was found, with cavity formation along grain boundaries and final sample failure.

ACKNOWLEDGEMENTS

This work was supported by the Project nº MAT2013-41233-R, Ministerio de Economía y Competitividad, España.

REFERENCES

[1] D.S. Wilkinson, C.H. Caceres and A.G. Robertson, Damage and Fracture Mechanisms During High-Temperature Creep in Hot-Pressed Alumina, *Journal of the American Ceramic Society*, **74**, 1991, pp. 922-933.

[2] J.D. French, M.P. Harmer, H.M. Chan and G.A. Miller, Coarsening-resistant dual-phase interpenetrating microstructures, *Journal of the American Ceramic Society*, **73**, 1990, pp. 2508-2510.

[3] F. Wakai and H. Kato, Superplasticity of TZP/Al_2O_3 Composite, *Advances in Ceramic Materials*, **3**, 1988 pp. 71-76.

[4] T.G. Nieh, J. Wadsworth and O.D. Sherby, *Superplasticity in metals and ceramics*, MI: Cambridge University Press, 1997.

[5] L.N. Satapathy and A.H. Chokshi, Microstructural Development and Creep Deformation in an Alumina–5% Yttrium Aluminum Garnet Composite, *Journal of the American Ceramic Society*, **88**, 2005, pp. 2848-2854.

[6] J.H. Lee JH, A. Yoshikawa, Y. Murayama, Y. Waku, S. Hanada and T. Fukuda, Microstructure and mechanical properties of $Al_2O_3/Y_3Al_5O_{12}/ZrO_2$ ternary eutectic materials, *Journal of the European Ceramic Society*, **25**, 2005, pp. 1411-1417.

[7] P.B. Oliete, J.I. Peña, A. Larrea, V.M. Orera, J. Llorca, J.Y. Pastor, A. Martín and J. Segurado, Ultra-high strength nanofibrillar Al_2O_3-YAG-YSZ eutectics, *Advances in Materials,* **19**, 2007, pp. 2313-2318.

[8] F.A. Huamán-Mamani, M. Jiménez-Melendo, M.C. Mesa and P.B. Oliete, Microstructure and high-temperature mechanical behavior of melt-growth $Al_2O_3/Er_3Al_5O_{12}/ZrO_2$ ternary eutectic composites, *Journal of Alloys and Compounds,* **536***,* 2012 pp. 527-531.

[9] A. Ikesue, T. Kinoshita, K. Kamata and K. Yoshida, Fabrication and Optical Properties of High-Performance Polycrystalline Nd:YAG Ceramics for Solid-State Lasers, *Journal of the American Ceramic Society*, **78**, 1995, pp. 1033-1040.

[10] J.P. Poirier, *Creep of Crystals*, Cambridge University Press, Cambridge, 1985.

[11] L. Changqing, W. Zhenting, A. Mingfu and Z. Hongbo, Interactions between Y_2O_3-Al mixture studied by solid-state reaction method, *Vacuum*, **87**, 2013, pp. 7–10.

[12] E. Souza, L.H. Leme, R. Freitas, J. Campos, R. Avillez and C. Costa, Processing and characterization of Al_2O_3 yttrium aluminum garnet powders, *Journal of Materials Research and Technology*, **2**, 2013, pp. 18–23.

[13] C.W. Won, H.H. Nersisyan, H.I. Won, J.H. Lee, K.H. Lee, Efficient solid-state route for the preparation of spherical YAG:Ce phosphor particles, *Journal of Alloys and Compounds*, **509**, 2011, pp. 2621–2626.

[14] P.B. Oliete, M.C. Mesa, A. Larrea and V.M. Orera, Directionally Solidified Al_2O_3–$Er_3Al_5O_{12}$–ZrO_2 Eutectic Ceramics with Interpenetrating or Nanofibrillar Microstructure: Residual Stress Analysis, *Journal of the American Ceramic Society*, 95, **2012**, pp. 1138–1146.

[15] M. Jiménez-Melendo, A. Domínguez-Rodríguez and A. Bravo-León, Superplastic Flow of Fine-Grained Yttria-Stabilized Zirconia Polycrystals: Constitutive Equation and Deformation Mechanisms, *Journal of the American Ceramic Society*, **81**, 1998, pp. 2761-2776.